IEEE Access
Multidisciplinary | Rapid Review | Open Access Journal

Received 12 June 2024, accepted 24 August 2024, date of publication 29 August 2024, date of current version 10 September 2024.

Digital Object Identifier 10.1109/ACCESS.2024.3451483

RESEARCH ARTICLE

CSI-RSRP-Based Unnecessary Handover Mitigation Through Linear Regression in Dynamic 5G NR Environments

SUNIL MATHEW[1], ELEONORA OLIOSI[1], LUCA DAVOLI[1], (Member, IEEE), NICOLÒ STROZZI[2], ANDREA NOTARI[2], (Member, IEEE), AND GIANLUIGI FERRARI[1], (Senior Member, IEEE)

[1]Department of Engineering and Architecture, University of Parma, 43124 Parma, Italy
[2]ASK Industries S.p.A., 42124 Reggio Emilia, Italy

Corresponding author: Luca Davoli (luca.davoli@unipr.it)

This work was supported in part by ASK Industries S.p.A., which allowed the use of the presented experimental data.

ABSTRACT 5G New Radio (NR), introduced in 2019 in the 3rd Generation Partnership Project (3GPP) Release 15, has become the global radio standard for 5G networks. Because of the presence of an increasing number of available 5G gNodeBs (gNBs), HandOver (HO) management is crucial, especially in terms of Quality of Service (QoS) and Quality of Experience (QoE) perceived by a User Equipment (UE). Unnecessary HandOvers (UHOs) cause latency peaks (on the order hundreds of milliseconds) and multiple throughput drops in 5G communications. In this paper, we first carry out an experimental campaign to investigate the behaviour of latency and throughput in correspondence to UHOs. Then, on the basis of a Matlab-based 5G NR DownLink (DL) transmission simulator, we propose an innovative linear regression-based algorithm to avoid UHOs, which relies on Channel State Information-Reference Signal Received Power (CSI-RSRP) measurements.

INDEX TERMS 5G new radio (NR), handover, latency, reference signal received power (RSRP), throughput.

I. INTRODUCTION

Nowadays, 5G New Radio (NR) is widely recognized as being the global standard for the air interface of 5G networks. It has been introduced with Release 15 (2019) [1] by the 3rd Generation Partnership Project (3GPP) during the so-called Phase 1 standardization. The 5G standard has been subsequently improved through Release 16 (2020), which expands and reinforces the 5G technology in areas of particular interest (such as Industry 4.0 and autonomous driving), and Release 17, initially planned for 2021 and then rescheduled for 2022, containing new 5G enhancements.

It is well known that the development of Intelligent Transportation Systems (ITSs) can greatly benefit from 5G communications. Exploiting 5G Ultra-Reliable Low Latency Communication (URLLC) [2] is crucial, since services to be offered by ITSs may be related to emergency brake warning, traffic jam warning, hazardous location warning, speed harmonization, lane change warning, vulnerable road user warning, etc [3]. In these scenarios, a service interruption (even for a few hundreds of milliseconds) would be critical.

In urban scenarios, a large amount of 5G gNodeBs (gNBs) is foreseen, with their overlapped network coverage regions possibly leading mobile User Equipments (UEs) to experience multiple (often unnecessary and very short) HandOvers (HOs) during their movements. Hence, HO management becomes a key design challenge because of the high data demand in future cellular networks. As discussed in [4], the HO process can be managed by letting a UE measure the Reference Signal Received Power (RSRP) values of neighbouring cells and, consequently, connect to the gNB with the highest RSRP. Unfortunately, this mechanism has disadvantages, such as latency increase and throughput drop, in the presence of Unnecessary HandOvers (UHOs) [5], i.e.,

The associate editor coordinating the review of this manuscript and approving it for publication was Jjun Cheng.

when a UE-gNB link is associated with the highest RSRP for a (too) short time after HO. Therefore, a gNB with a lower RSRP but a longer stable connection should be preferred in order to avoid local UHOs which worsen users' Quality of Service (QoS) and Quality of Experience (QoE).

In the literature, the problem of UHOs is well known and tackled. In [6], an approach based on the so-called UE's Time of Stay (ToS) measurement, with consequent setting of a critical time threshold, is presented and applied to Heterogeneous Networks (HetNets). In detail, this critical time threshold ensures that the UE connects to a serving cell with sufficiently high signal level for a sufficiently long time and, therefore, the HO is estimated to be reliable. According to [7], the HO for femtocells is performed only if (i) the Received Signal Strength (RSS) is higher than a predefined threshold for a certain amount of time and (ii) the bandwidth supported by the potential serving cell is sufficient. Another UHO management approach between a macrocell and a femtocell in a WiMAX network is presented in [8], taking into account (among other requirements on the serving cell bandwidth and the measured RSS level) the UE speed, which must be below a critical threshold so that the UE can correctly perform the HO.

Recently, there is an increasing interest on the development of 5G NR simulators, which allow to investigate 5G NR performance. Relevant examples are 5G LENA [9], a NR system-level module of the discrete-event network simulator ns-3 [10] including full protocol stack and end-to-end implementations, and 5G-air-simulator [11], an open source C++ simulator implementing several network architectures with multiple cells and users, and different mobility and application models. Although these existent simulators are fairly flexible, in order to effectively investigate mechanisms to be adopted to optimize the UHOs, we develop a novel Matlab-based 5G NR DownLink (DL) transmission simulator, exploiting experimental 5G data to make the identification (and, possibly, avoidance) of potential UHOs accurate.

This work represents a significant extension of [12], where a preliminary 5G NR DL transmission simulator development was described and its application to HO management was considered by simply the simulated performance with experimental results. The novel contributions of this paper relate, first, to the collection of experimental measurements of throughput and service latency values in a dynamic 5G environment. In fact, it has been observed that throughput drops and latency peaks take place when the mobile UE hands-over for a very short time from one gNB to another gNB—namely, during UHOs. On the basis of the obtained experimental results and through the use of an extended version of the 5G NR DL transmission simulator presented in [12], the second novel contribution of this paper is the development of an HO management approach aimed at avoiding the UHOs. Typically, the serving gNB is selected as the one providing the highest instantaneous Channel State Information-Reference Signal Received Power (CSI-RSRP) value at each measurement point: in this case, UHOs correspond to isolated peaks of the measured CSI-RSRPs. In order to avoid this phenomenon, linear regression is applied to the CSI-RSRP values from neighboring gNBs: the selected gNB is the one with the highest linear regression-based predicted RSRP. As a consequence, the proposed HO management algorithm eliminates isolated CSI-RSRP peaks, thus significantly reducing UHOs.

For the sake of clarity, in Table 1 we list the acronyms adopted in this paper, for convenience.

TABLE 1. List of the acronyms adopted in the manuscript.

3GPP	3rd Generation Partnership Project
AI	Artificial Intelligence
ANN	Artificial Neural Network
BPSK	Binary Phase-Shift Keying
BER	Bit Error Rate
CI	Confidence Interval
CSI-RS	Channel State Information Reference Signal
CSI-RSRP	Channel State Information-Reference Signal Received Power
DL	DownLink
EVB	EValuation Board
FNN	Feedforward Neural Network
gNB	gNodeB
GNSS	Global Navigation Satellite System
GTB	Gradient Tree Boosting
HO	HandOver
k-NN	k-Nearest Neighbors
ITS	Intelligent Transportation System
LOS	Line-Of-Sight
LSTM	Long Short Term Memory
NLOS	Non-Line-Of-Sight
NN	Neural Network
NR	New Radio
NZP	Non-Zero Power
MAE	Minimum Absolute Error
ML	Machine Learning
PL	Path Loss
PSS	Primary Synchronization Signal
SVR	Support Vector Regression
QoE	Quality of Experience
QoS	Quality of Service
RE	Resource Element
RF	Random Forest
RMa	Rural Macrocell
RS	Reference Signal
RSRP	Reference Signal Received Power
RSS	Received Signal Strength
SIM	Subscriber Identification Module
SINR	Signal-to-Interference-plus-Noise Ratio
SMA	SubMiniature version A
SS	Synchronization Signals
SSS	Secondary Synchronization Signal
TDL	Tapped Delay Line
UAV	Unmanned Aerial Vehicle
UE	User Equipment
UHO	Unnecessary HandOver
UMa	Urban Macrocell
UMi	Urban Microcell
URLLC	Ultra-Reliable Low Latency Communication
ZP	Zero Power

The rest of this paper is organized as follows. In Section II, an overview on how HO problems have been discussed in the literature is presented. Section III presents key 5G NR basics. In Section IV and Section V, the experimental setup for the performance campaign and the obtained results, in terms of latency and throughput, are discussed, respectively. In Section VI, the development of our Matlab-based 5G

NR simulator is illustrated. Section VII is dedicated to HO management: in Subsection VII-A, the UHOs problem in a 5G NR dynamic environment is introduced, whereas in Subsection VII-B our novel RSRP-based linear regression approach to avoid UHOs is proposed. In Section VIII, conclusions are drawn.

II. RELATED WORKS

A. HO PROBLEMS

As detailed in [13], an HO takes place when a moving UE is forced to change its serving cell in its connected mode: since the UE switches from one serving cell to another, data transmission may then be disrupted, thus degrading both QoS and QoE. Therefore, managing HOs becomes of paramount importance, especially when dealing with networks with many cells. In fact, when the number of experienced HOs increases, the probability of connection failure increases as well. Moreover, multiple and really short HOs, possibly happening in an ''intersection area'' potentially covered by multiple gNBs, turn out to be extremely detrimental for network performance, besides being (most of the time) also unnecessary for cellular coverage purposes.

A particular class of UHOs is represented by ''ping-pong'' HOs [14], corresponding to situations where a UE rapidly switches between two serving cells within a short time period, thus generating unnecessary signaling overhead at the gNBs and degrading QoE and QoS for the other UEs. Therefore, unnecessary ''ping-pong'' HOs (likely taking place in dense and highly mobile networks) should be mitigated as much as possible (ideally, eliminated).

Focusing on an HO procedure, three different stages can be identified: (i) HO information gathering, (ii) HO decision, and (iii) HO execution [15]. In detail, during the *first* stage the different available gNBs and their main attributes are detected. Subsequently, in the *second* stage the best network to be connected to is chosen according to proper criteria—as an example, RSS, Bit Error Rate (BER), and Signal-to-Interference-plus-Noise Ratio (SINR). Finally, in the *last* stage the connection with the new gNB is established, while the connection with the previous gNB is released. Among the above stages, special attention needs to be paid to the decision stage (when the UE identifies its next serving cell), to make the HO successful and to avoid degradation of QoS and QoE. This underlines the importance of properly evaluating and choosing representative parameters (e.g., RSS) in HO algorithms.

B. HO PROBLEMS MITIGATION

In the literature, the HO management problem in a dynamic cellular environment can be addressed relying on Artificial Intelligence (AI) and Machine Learning (ML) algorithms. In [16], various Neural Network (NN)-based approaches for HO forecasting are compared. Similarly, a cascade of NNs—a Long Short Term Memory (LSTM) and a Feedforward Neural Network (FNN)—is used in [17]: *first*, to predict future RSRP values; *then*, to classify an HO event either as HO success or failure. In [18], after a RSRP-based time series prediction exploiting a LSTM network, a classifier is used to evaluate if an HO trigger event is about to take place.

Focusing on RSRP prediction, AI and ML approaches can be found in the literature. In [19], different regression methods are used to predict (in an Unmanned Aerial Vehicle (UAV) environment) the RSRP value as a function of the distance between the serving gNB and the drone and of the elevation angle. In [20], the RSRP values are predicted in a UAV environment exploiting an Artificial Neural Network (ANN) fed with nine inputs (namely: drone's latitude, longitude, ground elevation, and altitude; network cell's latitude, longitude, and ground elevation; cell's building and antenna height). In [21], this approach is refined using an Ensemble Learning (EL) method [22] for RSS prediction—more precisely, combining k-Nearest Neighbors (k-NN), Support Vector Regression (SVR), Random Forest (RF), AdaBoost, and Gradient Tree Boosting (GTB).

III. 5G NR BASICS

A. SYNCHRONIZATION SIGNALS(SSs)

The Synchronization Signalss (SSs) can be categorized as: Primary Synchronization Signal (PSS) and Secondary Synchronization Signal (SSS).

- The PSS is generated starting from a sequence computed through a cyclic code with the cell ID as initial parameter [23], is used by the UE for DL frame synchronization, and allows to recover the position of the first symbol in a radio frame. The cell ID, denoted as $N_{\mathrm{ID}}^{\mathrm{cell}}$, is an integer number in $\{0, 1, \ldots, 1007\}$ calculated as follows:
$$N_{\mathrm{ID}}^{\mathrm{cell}} = 3N_{\mathrm{ID}}^{(1)} + N_{\mathrm{ID}}^{(2)} \quad (1)$$
where $N_{\mathrm{ID}}^{(1)} \in \{0, 1, \ldots, 335\}$ and $N_{\mathrm{ID}}^{(2)} \in \{0, 1, 2\}$, with $N_{\mathrm{ID}}^{(2)}$ and $N_{\mathrm{ID}}^{(1)}$ being recovered from the PSS and the SSS, respectively.
- The SSS is generated from a sequence computed through a cyclic code (as the PSS), is transmitted using Binary Phase-Shift Keying (BPSK) [23], and is also used by the UE for DL frame synchronization.

B. CHANNEL STATE INFORMATION REFERENCE SIGNAL (CSI-RS)

The UE estimates the gNB-UE link channel quality via the DL-only Channel State Information Reference Signal (CSI-RS) signal. The standard [24] distinguishes between Non-Zero Power (NZP) CSI-RS and Zero Power (ZP) CSI-RS. NZP CSI-RS is used at the UE to: (i) measure the received power in order to manage beams and mobility; (ii) acquire DL CSI; (iii) measure interference; and (iv) track time and frequency. On the contrary, given that no power is transferred in this resource, ZP CSI-RS is mainly used for interference monitoring.

With the aim of estimating the channel quality, various quality metrics associated with the CSI-RS can be defined.

Among them, we introduce the CSI-RSRP. According to the 3GPP specifications [25], this metric corresponds to "*the linear average over the power contributions (in [W]) of the Resource Elements (REs) of the antenna port(s) that carry CSI reference signals configured for RSRP measurements within the considered measurement frequency bandwidth in the configured CSI-RS occasions.*" The CSI-RSRP, denoted as ρ (dimension: [W]), can thus be computed as follows:

$$\rho = \frac{1}{K}\sum_{k=1}^{K} P_{\mathrm{rs},k} \tag{2}$$

where: K is the total number of Reference Signal (RS) REs; and $P_{\mathrm{rs},k}$ is the estimated received power (dimension: [W]) in the k-th ($k = 1, \ldots, K$) RS RE.

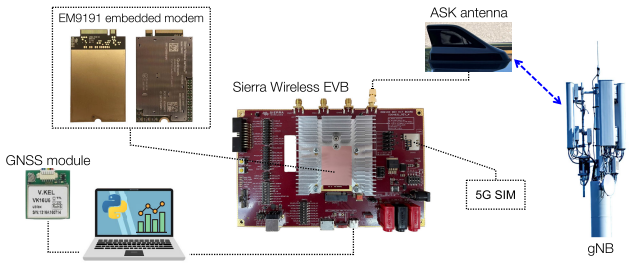

FIGURE 1. Block diagram of the experimental testbed.

The evaluation of CSI-RSRP allows to (i) select cells, (ii) manage mobility and HO, and (iii) manage beams. In the following, we take into account the CSI-RSRP measurements on an NZP CSI-RS RE.

IV. EXPERIMENTAL DATA COLLECTION IN A MOBILE SCENARIO

In order to implement a realistic 5G NR DL transmission simulator (detailed in Section VI), an experimental data collection (through an *on-field* campaign) in a mobile scenario, performed in the industrial area of Reggio Emilia, Italy, was expedient to collect reference CSI-RSRP measurements.

A Sierra Wireless EM9191 5G EValuation Board (EVB) embedded wireless modem, hosting a Subscriber Identification Module (SIM) card of the 5G provider of the considered gNB, connected to an antenna (developed by ASK Industries S.p.A [26] and mounted on the top of the car to connect to the gNB itself) are the components of the used experimental testbed, whose block diagram is shown in Figure 1. A SubMiniature version A (SMA) cable is used to connect the antenna with the EVB. A Type-C cable with serial communication is then used to connect the EVB to a laptop. RSRP readings have been monitored and gathered using AT commands of the Sierra Wireless modem. The coordinates related to the RSRP measurements have also been gathered using a Stemedu Vk-162 Global Navigation Satellite System (GNSS) module.

Overall, the following data were experimentally gathered: (i) cell ID $N_{\mathrm{cell}}^{\mathrm{ID}}$ (as in Eq. (1)), which corresponds to the NR physical cell ID of the serving cell and is associated with the gNB the 5G modem (i.e., the UE) is connected to (while inside the moving car); (ii) CSI-RSRP measurements from all "perceived" gNBs (including the one which the 5G modem is actually connected to); and (iii) coordinates (latitude, longitude) of the associated CSI-RSRP measurements points—the distances between gNBs and UE are computed using these coordinates, under the implicit assumption of perfect knowledge of the gNBs' positions.

The anticipated mobile UE path and the gathered CSI-RSRP data are displayed in Figure 2. The path, shown as a blue line, has been selected in order to ensure Line-Of-Sight (LOS) conditions between the reference UE and the connected gNB, while the UE was carried in a vehicle traveling away from the gNB at an average speed equal to 60 km/h. The experimentally acquired CSI-RSRP is represented, in terms of height and color, on top of the bi-dimensional path. In Subsection VI-D, these empirically obtained values will be compared with simulation-based ones.

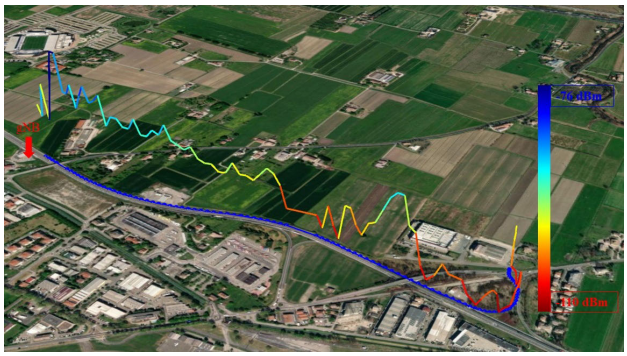

FIGURE 2. Experimental RSRP: the height (with respect to the bi-dimensional path) and the color are representative of the measured RSRP. The blue line indicates the corresponding path of the UE.

V. LATENCY AND THROUGHPUT EXPERIMENTAL EVALUATION

In order to evaluate the impact on latency and throughput of UHOs, additional tests were carried out. These tests included latency analysis with different DL throughput values. In 5G systems, the expected target interruption time during HO is, *in principle*, 0 ms, but the UE may experience, *in practice*, an interruption time on the order of hundreds of milliseconds. This service interruption, caused by no data plane traffic, requires temporary data storage in a buffer in the UE. Moreover, multiple services running in the UE lead to an additional latency. For the purpose of replicating the latency due to temporary data storage, data traffic patterns with the following DL throughput were created: 0 Mbps (no DL data is transmitted, the latency is estimated using the `ping` command), 10 Mbps, 100 Mbps, and maximum allowed data rate (i.e., no limits set on the DL throughput).

To this end, PHY-layer performance metrics can be retrieved using the 5G modem, while measuring the

communication throughput requires to opt for an application layer approach. In this manuscript, the `iperf3` [27] tool has been used (as further discussed on Section V) to measure the throughput, generating data traffic by properly setting the bandwidth value. Then, in order to measure the communication delay, we opt for using the simple `ping` command (which exploits ICMP at network layer). More in detail, `iperf3` is a network tool used for active measurements of the maximum achievable bandwidth on IP networks, renowned for its tuning support of different timing and buffer parameters, as well as of several network protocols. Then, `iperf3` and `ping` servers were set up at the University of Parma. Measuring the latency at the PHY layer would be more accurate, but the analysis above is more realistic from a user experience perspective. Moreover, evaluating the performance degradation due to HO at the network layer is more relevant to predict the behaviour of a realistic IP-based information flow.

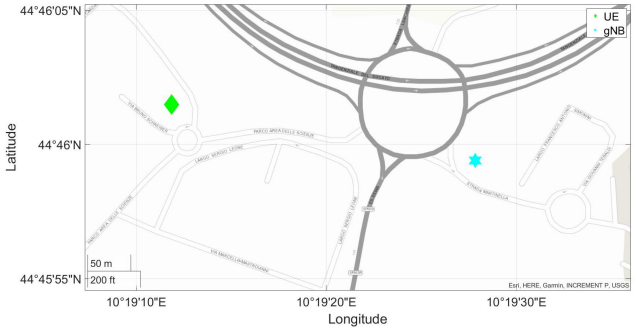

FIGURE 3. Geographical location of the gNB (blue marker) and the UE (green marker) for testing the performance in stationary condition.

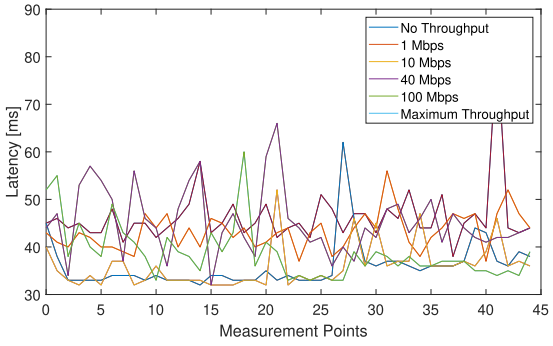

FIGURE 4. Latency for various DL throughput values while the UE is stationary (as shown in Figure 3).

The preliminary experiment aimed at evaluating the latency with different DL throughput values, with gNB (blue marker) and UE (green marker) placed as shown in Figure 3. The (fixed) distance between gNB and UE was 370 m and the observed RSRP was between −85 dBm and −95 dBm. In Figure 4, the throughput is shown as a function of the measurement points (corresponding to time instants): it can be observed that the artificial DL data traffic has no impact on the latency. Table 2 shows the average latency (dimension: [s]) for the considered DL throughput values, with highest DL throughput equal to 324 Mbps.

TABLE 2. Average latency for different DL throughput values while the UE is stationary.

Throughput [Mbps]	Average Latency [ms]
0	46.26
1	36.11
10	43.26
40	35.97
100	45.31
324 (max)	38.84

In order to identify the effect of UHOs on latency and throughput, multiple tests were carried out by selecting the reference path shown in Figure 6—this path has been chosen as one would expect multiple HOs due to multiple gNBs, within connection range, shown in Figure 5.

The first experiment aimed at analysing the latency performance when there is no artificial data traffic and there are multiple HOs. Figure 7 shows the connection behaviour over the map: different colors represent connectivities to different gNBs (each one identified by a specific value of the cell ID $N_{\text{cell}}^{\text{ID}}$). It can be observed that the UE is connected to some gNBs for (very) short durations. In Figure 8, the latency is shown as a function of the measurement point: the latency is lower than 60 ms in correspondence to most of the measurement points, with sporadic peaks due to HOs. However, even if there are some UHOs, this does not have a relevant impact as the maximum observed latency is 173 ms. It can be observed that performance degradation occurs even if there is no HO; this is due to channel status' variation [28]. In Figure 9, the latency is shown together with the RSRP: it can be concluded that the latency is not affected by the RSRP along the considered reference path.

Another experiment was carried out by generating a data traffic of 10 Mbps. Figure 10 shows the connection behaviour over the map: the colored markers represent the identified cell IDs along the path. In Figure 11, multiple latency peaks can be observed, with values higher than 2000 ms. These critical peaks are due to UHOs, which could be avoided by using proper HO mitigation mechanisms. Figure 12 illustrates the impact of HOs on latency and RSRP: it can be concluded that HOs have a stronger impact on latency than on RSRP (as observed in Figure 12).

We carried out experimental tests also with a DL throughput equal to 100 Mbps. Figure 13 shows, on the map, the different cell IDs identified during the experiment. By comparing the results in Figure 13 with the results in Figure 10, it can be observed that the new cell ID $N_{\text{cell}}^{\text{ID}} = 730$ was identified during this trip. In Figure 14, the experimental latency peaks are similar to the case with a DL throughput equal to 10 Mbps. In Figure 15, the impact of HOs on latency and RSRP is shown: the obtained results show that the impact of the HOs is more significant on latency than on RSRP.

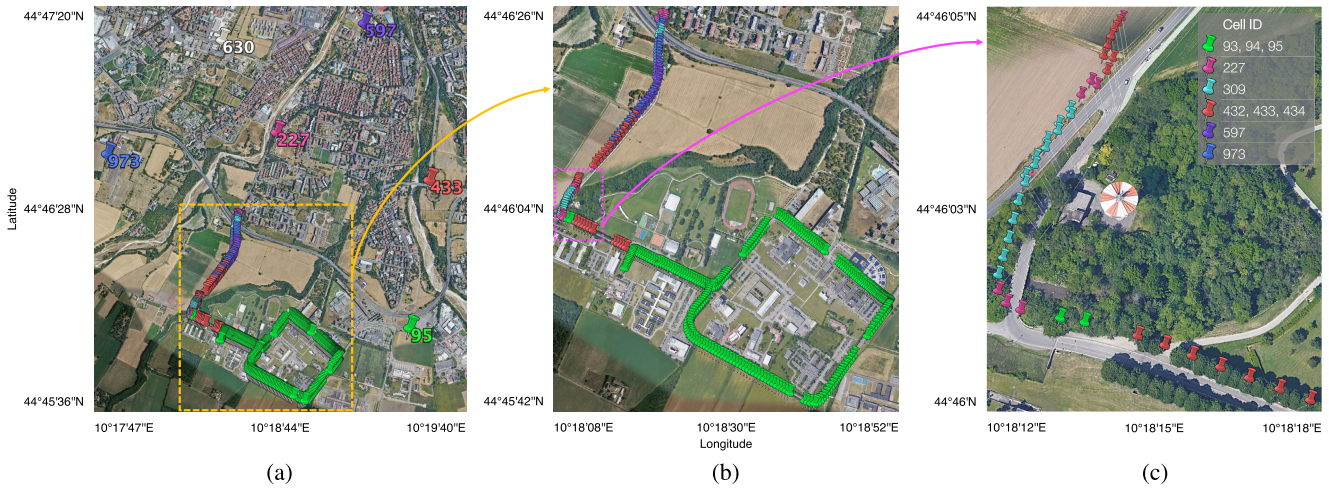

FIGURE 5. Map representation of the reference area, located in Parma, Italy, at the scientific campus of the University of Parma, identified for the experimental evaluation. Pins represent the measurement points, while colors represent different cell IDs N_{cell}^{ID}. Pins with names represent the different gNBs present in the area. The bottom region marked in pink shows an example of a region where multiple HOs occur.

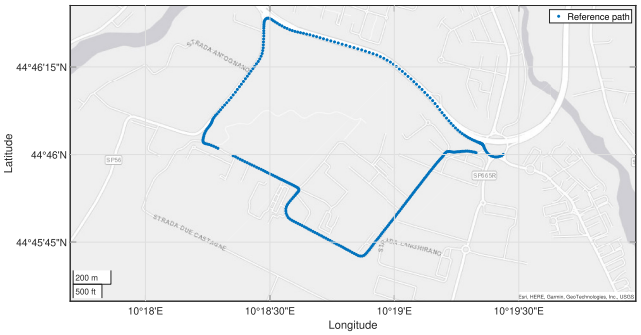

FIGURE 6. Reference path for the experimental trials.

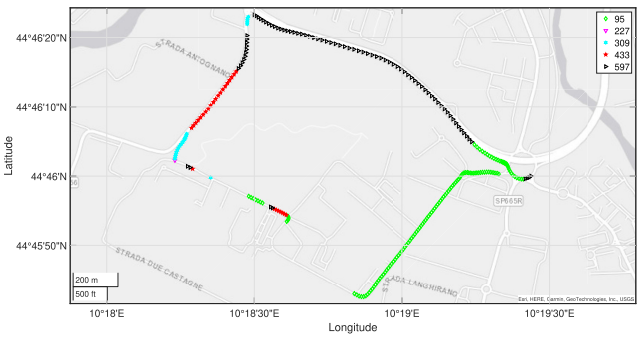

FIGURE 7. Map representation of the experimental results while the UE is moving along the test path without artificial data traffic. Markers represent the measurement points and colors represent the identified cell IDs.

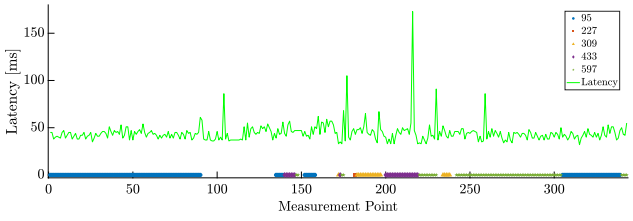

FIGURE 8. Experimental latency results while the UE is moving along the path shown in Figure 7 without artificial data traffic.

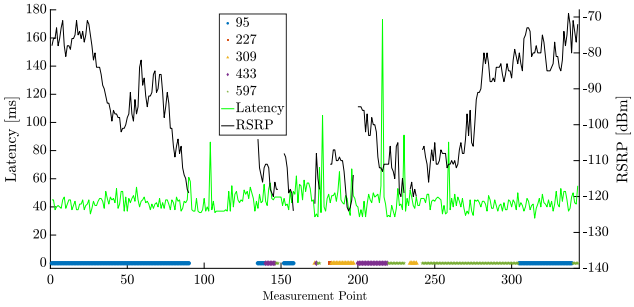

FIGURE 9. Experimental latency and RSRP results while the UE is moving along the path shown in Figure 7 without artificial data traffic. Left *y*-axis represents latency and right *y*-axis represents RSRP values.

In order to understand the impact on latency when the maximum DL throughput is considered, another experiment was conducted by setting unlimited bandwidth (i.e., no bandwidth constraint) in the `iperf3` tool. Figure 16 shows the path of the mobile UE with the associated cell IDs. In Figure 17, where the experimental latency measured along the path in Figure 16 is shown, it can be seen that there are peaks due to HOs. More precisely, the latency peaks are not as high as in the two previous cases (with DL throughput equal to 10 Mbps and 100 Mbps, respectively): this may be due to the fact that in previous cases there was a pre-set data bandwidth, whereas in this case the UE is using the maximum available bandwidth. In detail, when a 100 Mbps traffic load is set, the `ping` data will be queued once the 100 Mbps load is reached, whereas when the load is set to the maximum available, `ping` data will not be queued. Finally, the results in Figure 18 (where latency and RSRP are shown as functions of the measurement

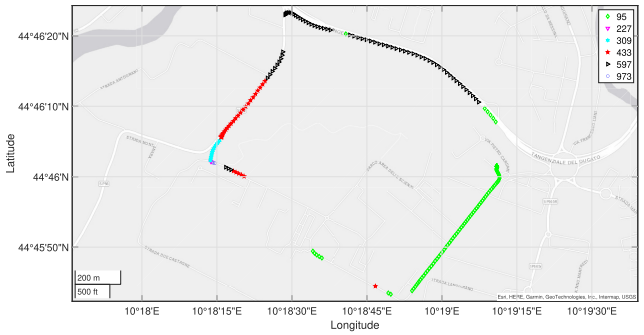

FIGURE 10. Map representation of the experimental results while the UE is moving along the test path with a DL throughput of 10 Mbps. Markers represent the measurement points and colors represent the identified cell IDs.

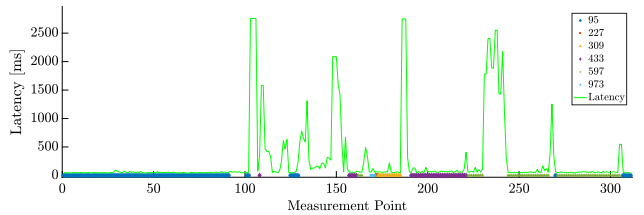

FIGURE 11. Experimental latency results while the UE is moving along the path shown in Figure 10 with a DL throughput of 10 Mbps.

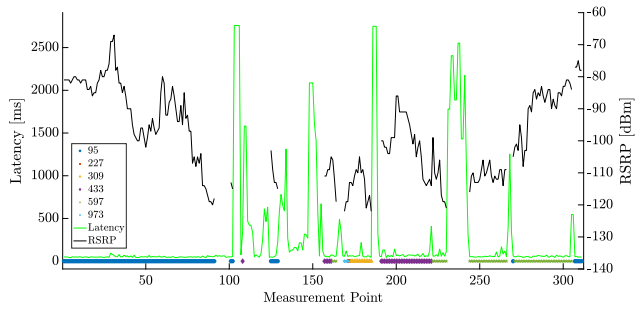

FIGURE 12. Experimental latency and RSRP results while the UE is moving along the path shown in Figure 10 with a DL throughput of 10 Mbps. Left y-axis represents latency and right y-axis represents RSRP values.

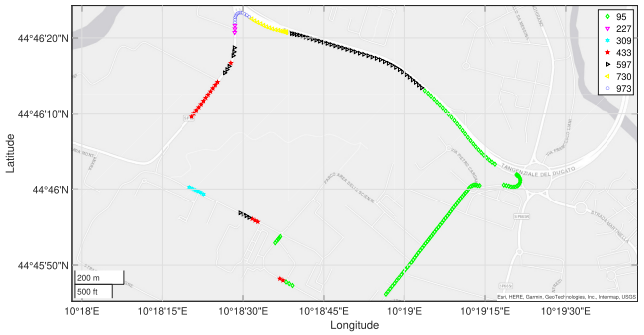

FIGURE 13. Map representation of the experimental results while the UE is moving along the test path with a DL throughput of 100 Mbps. Markers represent the measurement points and colors represent the identified cell IDs.

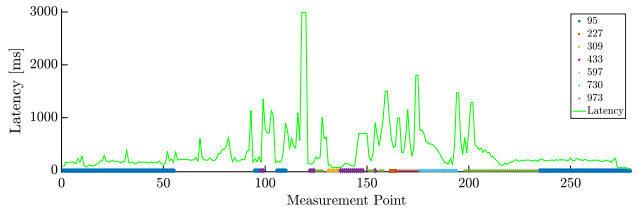

FIGURE 14. Experimental latency results while the UE is moving along the path shown in Figure 13 with a DL throughput of 100 Mbps.

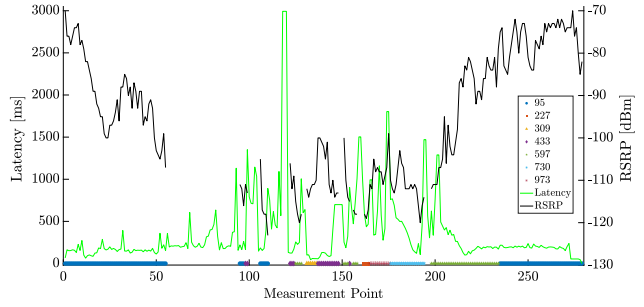

FIGURE 15. Experimental latency and RSRP results while the UE is moving along the path shown in Figure 13 with a DL throughput of 100 Mbps. Left y-axis represents latency and right y-axis represents RSRP values.

points) corroborate the fact that the latency is more affected by HOs than RSRP.

The previously described experiments are instrumental to identify the impact on latency of RSRP, HOs, and different DL throughput values while the UE is moving along a reference path. In Figure 19, we show the throughput and RSRP over the reference path: the markers with different colors refer to different cell IDs. The throughput drops are due to the fact that there is no data plane traffic during HOs. In Figure 20, it can also be observed that the DL throughput is correlated to the RSRP: the correlation coefficient between downlink throughput and RSRP is equal to 0.716. Therefore, as mentioned before, the performance degradation occurring even in the absence of HOs is caused by a change in the channel conditions.

From the results in the previous experiments, it can be concluded that there are UHOs, as different cell IDs appear in different experiments: in other words, it seems that the UE connects to gNBs in an irregular way. It can also be observed that there is a throughput drop during each HO: while necessary HOs cannot be avoided, UHOs should be removed. Finally, we remark that UHOs typically occur near bridges, intersections, roundabouts and traffic signals: this suggests that 5G-based devices in ITSs should be carefully designed.

VI. 5G NR SIMULATOR

As anticipated in Section IV, the experimental data collected on the field in a mobile scenario are instrumental to develop an accurate software simulator, in order to test the designed

UHO mitigation strategies. More in detail, Matlab and its 5G Toolbox are adopted to implement our 5G NR simulator.

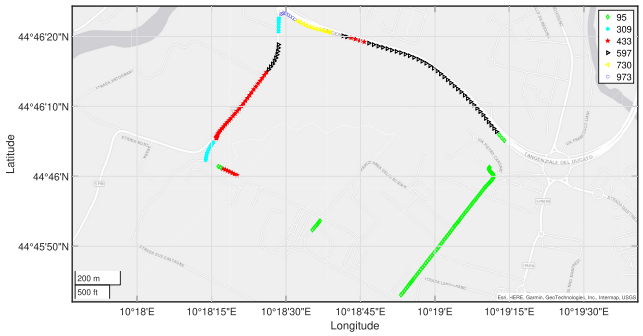

FIGURE 16. Map representation of the experimental results while the UE is moving along the test path with maximum DL throughput. Markers represent the measurement points and colors represent the identified cell IDs.

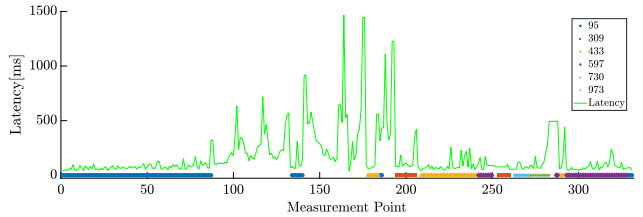

FIGURE 17. Experimental latency results while the UE is moving along the path shown in Figure 16 with maximum DL throughput.

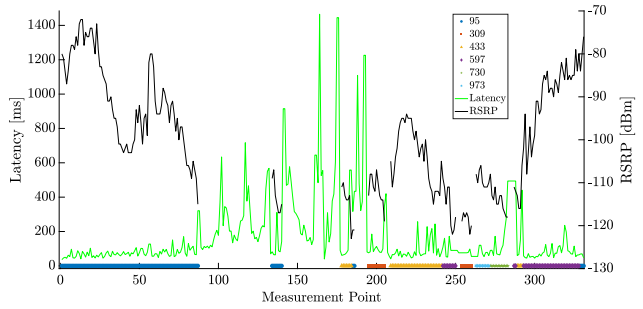

FIGURE 18. Experimental latency and RSRP results while the UE is moving along the path shown in Figure 16 with maximum DL throughput. Left *y*-axis represents latency and right *y*-axis represents RSRP values.

A. SIMULATION PARAMETERS

First, a 5G NR waveform is created, including 1 SS burst and 1 NZP CSI-RS resource, with the SS burst being transmitted at a proper power. The values of relevant parameters are shown in Table 3.

B. CHANNEL MODEL

A Tapped Delay Line (TDL) channel model is identified as the most appropriate channel profile for our simulator, since it considers both multi-path propagation and fading. The 3GPP standard envisions five different TDL channel

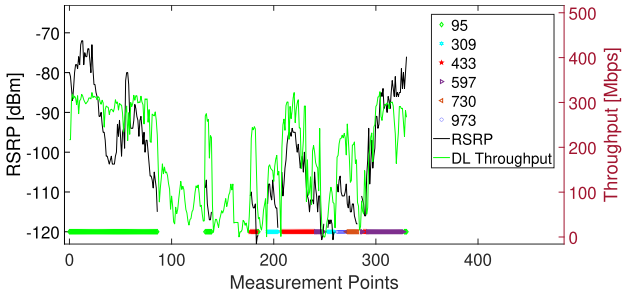

FIGURE 19. Experimental throughput while the UE is moving along the path shown in Figure 16. Left *y*-axis represents RSRP and right *y*-axis represents throughput.

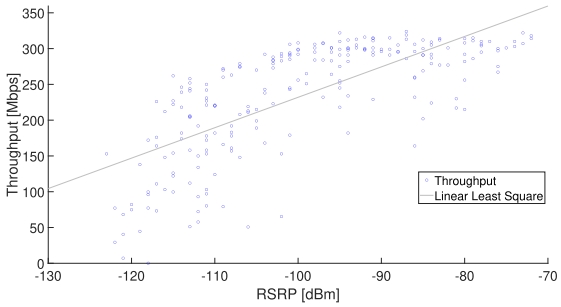

FIGURE 20. Experimental throughput of the moving UE on the path shown in Figure 16. The scatter points indicate the DL throughput. The straight line represents the linear least-squares fit.

TABLE 3. Simulation parameters.

Parameter	Value
$N_{\text{cell}}^{\text{ID}}$	117
N_{FFT}	2048
Δf	15 kHz
f_c	3.5 GHz
f_s	30.72 MHz
SS burst power	17.2 dBm
P_{TX}	45 dBm
H_{TX}	30 m
H_{RX}	1.5 m
v	60 km/h
T_{RX}	290 K
F_{RX}	6 dB

profiles [29]: three TDL profiles (namely, TDL-A, TDL-B and TDL-C) are designed to account for three Non-Line-Of-Sight (NLOS) conditions, whereas two TDL profiles (namely, TDL-D and TDL-E) model LOS propagation conditions. An experimental evaluation of the propagation conditions of the communication link between the considered gNB ($N_{\text{cell}}^{\text{ID}} = 117$) and the mobile UE is needed to select the most appropriate TDL channel profile.

In order to model the channel by taking into account the movement of the UE, the following maximum Doppler shift f_D (dimension: [Hz]) needs to be considered:

$$f_D = f_c \cdot \frac{v}{c} \tag{3}$$

where v represents the speed of the mobile UE (dimension: [km/h]) and c indicates the speed of light ($c \simeq 1.08 \cdot 10^9$ km/h). By using the values of f_c and v in Table 3, it follows that $f_D = 194.58$ Hz

In addition to multi-path propagation, the Path Loss (PL) between the gNB and the mobile UE needs to be calculated to account for channel attenuation. According to the considered scenario (among: Urban Macrocell, UMa; Urban Microcell, UMi; Rural Macrocell, RMa), different PL models can be used for a 5G NR communication system [29]. These models vary, in their formulations, in terms of (as shown in Table 3): carrier frequency f_c (dimension: [GHz]); height of the transmitter H_{TX} (dimension: [m]); height of the receiver H_{RX} (dimension: [m]); and distance between gNB and UE (dimension: [km]). The industrial area in Reggio Emilia, Italy, considered in the experimental data campaign, is well modelled by the UMa scenario configuration. The specific TDL channel profile depends on the propagation conditions (LOS or NLOS) of the communication link between the gNB and the mobile UE. Therefore, the UMa-NLOS and UMa-LOS scenarios are considered.

C. CELL SEARCH AND CSI-RS MEASUREMENTS

At the UE, cell search is primarily carried out. In order to compute $N_{\mathrm{ID}}^{\mathrm{cell}}$ according to Eq. (1), PSS and SSS are extracted from the received SS burst. Then, the CSI-RSRP (dimension: [W]) is evaluated (in linear scale) as follows:

$$\rho_{\mathrm{lin}} = \left| \frac{\sum_{i=1}^{N_{\mathrm{RE}}^{\mathrm{CSI-RS}}} s_{\mathrm{CSI-RS}}^{(\mathrm{rec})}(i) \cdot (s_{\mathrm{CSI-RS}}^{(\mathrm{ref})}(i))^*}{N_{\mathrm{RE}}^{\mathrm{CSI-RS}}} \right|^2 \tag{4}$$

where: $N_{\mathrm{RE}}^{\mathrm{CSI-RS}}$ is the total number of CSI-RS REs; and $s_{\mathrm{CSI-RS}}^{(\mathrm{rec})}$ and $s_{\mathrm{CSI-RS}}^{(\mathrm{ref})}$ are the received and the reference CSI-RS symbols, respectively. The final RSRP value (in logarithmic scale) $\rho^{(\mathrm{sim})}$ (dimension: [dBm]) is then

$$\rho^{(\mathrm{sim})} = 10 \log_{10}(\rho_{\mathrm{lin}}) + 30\,. \tag{5}$$

D. RESULTS

We consider 100 simulation runs[1] and the average (over the simulation runs) RSRP value is computed at each position of the UE (at the corresponding distance from the gNB). The RSRP Confidence Interval (CI) at each distance is calculated as follows [30]:

$$CI = \theta \pm z^* \cdot \frac{\sigma}{\sqrt{n_{\mathrm{pop}}}} \tag{6}$$

where: θ is the sample mean; σ is the standard deviation of the population; n_{pop} is the population size (which corresponds to the number of simulation runs and, thus, is equal to 100); and z^* is the so-called *z-star parameter* and is set to 1.96 to compute the 95% CI [30].

[1]Our results show that this number of simulation runs is statistically sufficient to obtain accurate RSRP results.

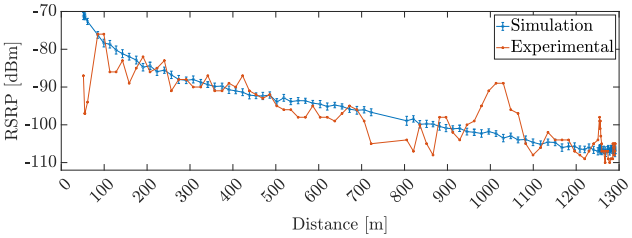

FIGURE 21. RSRP as a function of the distance between UE and gNB in the scenario characterized by the parameters in Table 3: average simulated (blue line with 95% CI bars) and experimental (orange line with asterisks) values are directly compared.

The PL model for the UMa-LOS scenario is chosen because the mobile UE is always in LOS conditions in the considered experimental scenario in Reggio Emilia, Italy.

The TDL profile can be either TDL-D or TDL-E, as mentioned in Subsection VI-B. We take into account both of them for cell search and RSRP measurements in order to identify the most accurate channel simulator, comparing the obtained results with the experimental ones. With both profiles, the correct cell ID $N_{\mathrm{cell}}^{\mathrm{ID}} = 117$ is detected from all the measurement points. Thus, the RSRP is measured on the received CSI-RS and the Minimum Absolute Error (MAE) value associated with each channel profile is calculated. It turns out[2] that the lowest MAE value is obtained with the TDL-D profile, which is then chosen in our simulator to simulate the transmission channel.

In Figure 21, the simulation-based CSI-RSRP $\rho^{(\mathrm{sim})}$ is shown (with its associated CI evaluated according to Eq. (6)) as a function of the distance between the gNB and the UE, together with the experimental values. It can be noticed that, despite some acceptable differences due to external factors that cannot be perfectly replicated in the simulator, simulated and experimental values are consistent. This motivates the use of our simulator to meaningfully test the performance of the proposed HO management strategy in the following.

VII. HO MANAGEMENT

A. UHO EXPERIMENTAL SETUP

In order to investigate the performance of the UHO mitigation strategy, which will be proposed in the following Subsection VII-B, we focus on the experimental setup. In order to do this, we rely on a supplementary experimental campaign in Parma, Italy, at the scientific campus of the University of Parma, as shown in Figure 5 (at multiple scales, zooming in from left to right). In particular, the pins represent measurement points during a vehicle trip: at each point, our embedded 5G modem is connected to a specific color-identified gNB. It can be observed that, in some portions of the path, multiple consecutive HOs happen. For instance, in the area shown in Figure 5c it can be seen that the UE carries out 7 HOs, with very short connection intervals per gNB. Each of these consecutive HOs introduces a

[2]The results are not shown here for conciseness.

non-negligible delay [31], which will consequently introduce a data transmission latency.

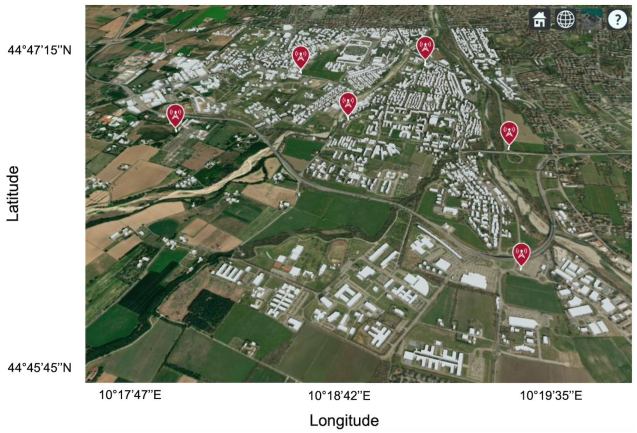

FIGURE 22. Map of the considered area obtained through the OpenStreetMap software. Red markers: gNBs. White markers: buildings.

Since at the scientific campus of the University of Parma the mobile UE can also be in NLOS conditions, a TDL-C channel profile is used to simulate NLOS conditions. The TDL-D model is kept to account for LOS conditions. Since a benchmark for the RSRP values in NLOS conditions was not available (as the experimental campaign in Reggio Emilia was carried out in LOS conditions), the method to identify the most suitable NLOS TDL channel profile for the simulator, mentioned in Subsection VI-D, cannot be implemented. The next steps of our procedure are the following. Six different gNBs are considered (those closest to our experimental campaign area) and, for each of them, the distances from our measurement points are calculated. The corresponding channel conditions are computed by means of the OpenStreetMap software [32], which allows to map the buildings and the obstacles in the considered geographical region, as shown in Figure 22. For the measurement points at distances longer than 2.5 km from the corresponding gNB and estimated to be in NLOS conditions, an RSRP value equal to -140 dBm is considered for the sake of computational efficiency.

In Figure 23, the results obtained simulating the RSRP values from the six different gNBs in the analysed area are shown. When considering the serving gNB as the one that provides the highest instantaneous RSRP, several "ping-pong" HOs (namely, a UE switches back and forth rapidly between two gNBs, as mentioned in II-A) take place. "Ping-pong" HOs can be observed even with the experimental RSRP values. More precisely, one can observe the appearance, in the experimental results, of a new cell ID value (namely, $N_{\text{cell}}^{\text{ID}} = 597$) that was not taken into account in the simulations because its gNB location was outside the considered geographical region for the simulations in Figure 22—OpenStreetMap only allows to consider a limited number of nodes in each map.

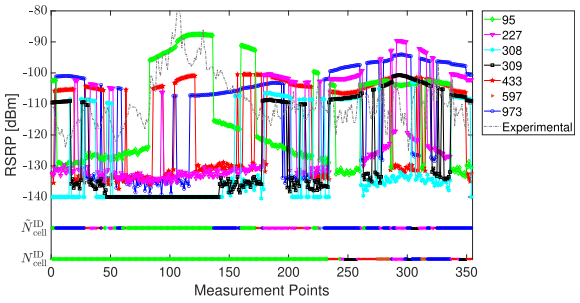

FIGURE 23. Simulation-based (solid lines with markers) and experimental (dashed line) RSRP values from the considered gNBs (with their cell IDs).

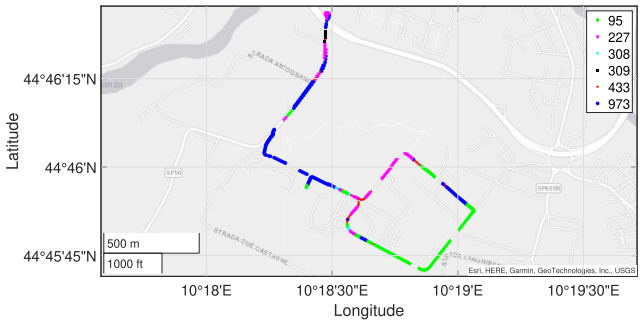

FIGURE 24. Simulation-based identification of cell ID $\tilde{N}_{\text{cell}}^{\text{ID}}$ identified by the mobile UE along the path considered in Figure 5 by instantaneous selection of the gNB with highest RSRP.

B. PROPOSED UHO MITIGATION MECHANISM

In order to avoid that the mobile UE hands-over from one gNB to another for a very short time interval (i.e., to avoid UHOs), as highlighted in Figure 23 and Figure 24, we have developed an approach based on the linear regression of the CSI-RSRP values. The used RSRP values, obtained through simulations as $\rho_{\text{gNB}}^{(\text{sim})}$, are the same considered in Subsection VII-A.

1) LINEAR REGRESSION

A general formula for polynomial regression is the following:

$$p(x) = p_0 + \sum_{i=1}^{n} p_i x^i \tag{7}$$

where n is the polynomial degree and $\{p_i\}_{i=1}^{n}$ are polynomial coefficients. For our purposes, we choose $n = 1$ in order to perform a linear regression in a least-square sense [33].

The pseudo-code representation of the proposed UHO mitigation mechanism, based on a sliding window approach, is shown in Algorithm 1. More precisely, we update the polynomial coefficients used for linear regression (namely, p_0 and p_1 in Eq. (7), for $n = 1$) over n_{obs} RSRP values (denoted as $\{\rho_{\text{gNB}}^{(\text{sim})}(x)\}$, where x is an observation epoch) related to the $n_{\text{gNB}} = 6$ considered gNBs. Then, we move the window every n_{pred} observations and evaluate the RSRP-based regression outputs (denoted as $\hat{\rho}_{\text{gNB}}^{(\text{sim})}$) for the next n_{pred}

points. Finally, in order to determine the cell ID $N_{\text{cell}}^{\text{ID}}$ which the UE is connected to (whose location is denoted as $\mathcal{U}_{\text{pos}}$), the number of occurrences of each cell is calculated in the n_{pred} observation interval: the most frequent cell is selected as candidate gNB to connect to, in order to avoid short (and useless) HOs, i.e., UHOs.

Algorithm 1 Proposed UHO Mitigation Mechanism

Require: $\rho_{\text{gNB}}^{(\text{sim})}$; n_{gNB}; n_{pred}; n_{obs}; $N_{\text{cell}}^{\text{ID}}$
Ensure: $\hat{N}_{\text{cell}}^{\text{ID}}(\mathcal{U}_{\text{pos}} : \mathcal{U}_{\text{pos}} + n_{\text{pred}})$
while true do
  for $i = 1 : n_{\text{gNB}}$ **do**
    Evaluate p_0 and p_1 over $\rho_{\text{gNB}_{(i)}}^{(\text{sim})}(\mathcal{U}_{\text{pos}} - n_{\text{obs}} : \mathcal{U}_{\text{pos}})$
    Estimate $\hat{\rho}_{\text{gNB}_{(i)}}^{(\text{sim})}(\mathcal{U}_{\text{pos}} + 1 : \mathcal{U}_{\text{pos}} + n_{\text{pred}})$
    $c_{\text{gNB}_{(i)}} = 0$ //counter variable
  end for
  for $x = \mathcal{U}_{\text{pos}} : \mathcal{U}_{\text{pos}} + n_{\text{pred}}$ **do**
    Compare $\hat{\rho}_{\text{gNB}}^{(\text{sim})}(x)$ among all considered gNBs
    Identify $\text{gNB}_{(j)} \leftarrow \max\left(\hat{\rho}_{\text{gNB}}^{(\text{sim})}(x)\right)$
    $c_{\text{gNB}_{(j)}} = c_{\text{gNB}_{(j)}} + 1$
  end for
  Identify $\text{gNB}_{(j)} \leftarrow \max(c_{\text{gNB}_{(j)}}) \quad \forall j \in [1 : n_{\text{gNB}}]$
  Estimate $\hat{N}_{\text{cell}}^{\text{ID}}(\mathcal{U}_{\text{pos}} : \mathcal{U}_{\text{pos}} + n_{\text{pred}})$ as $N_{\text{cell}}^{\text{ID}}(\text{gNB})$
end while

The RSRP-based linear regression results and the selected cell ID $\hat{N}_{\text{cell}}^{\text{ID}}$ are shown in Figure 25 (a) up to evaluation point 100 and (b) from point 300 to point 350, respectively, for all the six considered gNBs. In all cases, n_{obs} is set to 50 and n_{pred} is set to 5. It can be noticed that the number of performed HOs is considerably reduced with respect to Figure 23 in the same regions. In Figure 26, a more detailed comparison among (a) the $\hat{N}_{\text{cell}}^{\text{ID}}$ values obtained with our linear regression-based approach and (b) both the $\tilde{N}_{\text{cell}}^{\text{ID}}$ and $N_{\text{cell}}^{\text{ID}}$ values computed, respectively, without regression and by the experimental procedure, is carried out in the measurement interval from point 200 to point 300. One can observe that several really short HOs appearing in Figure 26(a) disappear in Figure 26(b) by using our approach.

Other (n_{obs}, n_{pred}) configurations have been considered. For instance, in Figure 27(a), the sliding window size is reduced to $n_{\text{obs}} = 10$ and is moved at every measurement point (namely, $n_{\text{pred}} = 1$). It can be observed that when taking into account a small regression interval (i.e., small values of n_{obs}), HOs of really short duration can still take place. On the other hand, in Figure 27(b), obtained using the configuration ($n_{\text{obs}} = 100$, $n_{\text{pred}} = 10$), one can notice that the number of performed HOs is considerably reduced, also with respect to Figure 26(b). Unfortunately, this configuration requires to collect a large number of measurements (namely, 100) before starting predicting the cell ID. Therefore, we consider the (n_{obs}, n_{pred}) = (50, 5) configuration as the most appropriate one for our purposes, because it represents a good *trade-off* between (i) performed HOs and avoided UHOs and (ii) computational complexity.

The results, in terms of selected values of the cell ID $\hat{N}_{\text{cell}}^{\text{ID}}$ obtained using our approach along the considered path, are shown in Figure 28: only 13 HOs are performed, which is smaller than both the 50 HOs obtained in simulations and the 19 HOs experimentally observed (in both cases without regression) shown in Figure 23.

2) ALTERNATIVE APPROACHES

As mentioned in Subsection II-B, alternative approaches for RSRP prediction have been proposed in the literature. For instance, various regression algorithms are explored in [19] to evaluate future RSRP values as functions of (i) the distance between the gNBs and a flying drone and (ii) the corresponding elevation angle. Unfortunately, a fair comparison between these methods and our proposed approach cannot be carried out since in our scenario, at each measurement point, the distance between the considered gNBs and the UE is available only in the simulation. Nevertheless, in order to demonstrate the quality of our proposed linear regression-based approach, we have adapted our RSRP prediction algorithm to consider also the distances between the UE and the potential serving gNBs. As a benchmark, the results (in terms of predicted cell ID $\hat{N}_{\text{cell}}^{\text{ID}}$) in the measurement interval from point 200 to point 300 are considered, as previously shown in Figure 26(b). The comparative results, obtained with a second-order polynomial regression, are shown in Figure 29: it can be observed that, considering the same interval as for Figure 26(b), in Figure 29 many more HOs happen, with the moving UE jumping from one gNB to another one many more times than by using our proposed approach.

On the other hand, in Figure 30 the application of a logarithmic model to predict the RSRP values used to identify the cell ID $\hat{N}_{\text{cell}}^{\text{ID}}$ is shown. Looking at these results, it can be concluded that the behaviour (in terms of HOs) is similar to that obtained by applying our proposed linear regression-based approach. Therefore, (i) knowing the distance between the moving UE and the potential serving gNB and (ii) applying a more complex regression model, do not lead to a significant performance improvement (in terms of $\hat{N}_{\text{cell}}^{\text{ID}}$ values) with respect to our proposed RSRP-based linear regression approach. It can be concluded that our approach can be considered the most computationally efficient, the easiest to implement, and, therefore, the one with the highest ratio between performance and complexity.

Besides the RSRP-based regression approaches mentioned above, other methods based on NN could be effective in managing the HO process, as mentioned in Section I. Unfortunately, the characteristics of the available dataset were not compatible with a NN-based approach. The limited amount of observations (only 354 measurement points) and the unbalanced representation of the six different cell IDs make NN training really inaccurate. As a matter of fact, cell ID values 308 and 309 appear much less, in the dataset, than cell ID values 95 and 973, as it can be observed in

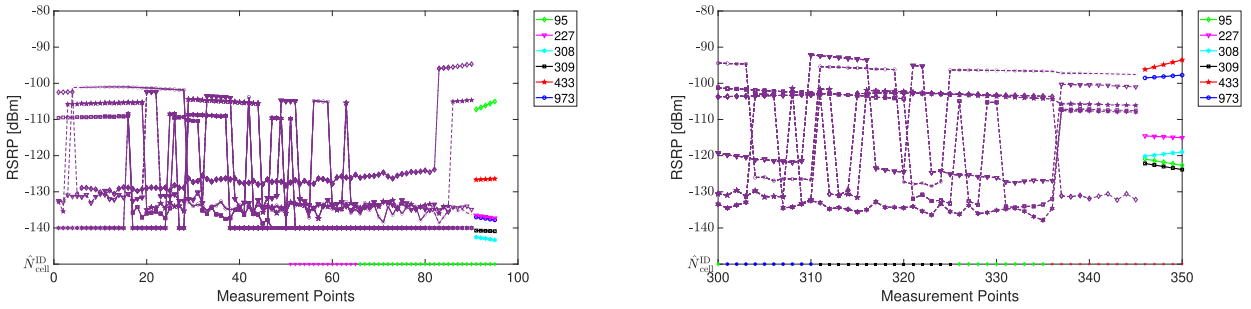

FIGURE 25. RSRP-based linear regression algorithm $\hat{N}_{\text{cell}}^{\text{ID}}$ results ($n_{\text{obs}} = 50$, $n_{\text{pred}} = 5$): (a) from 1 to 100; and (b) from 300 to 350.

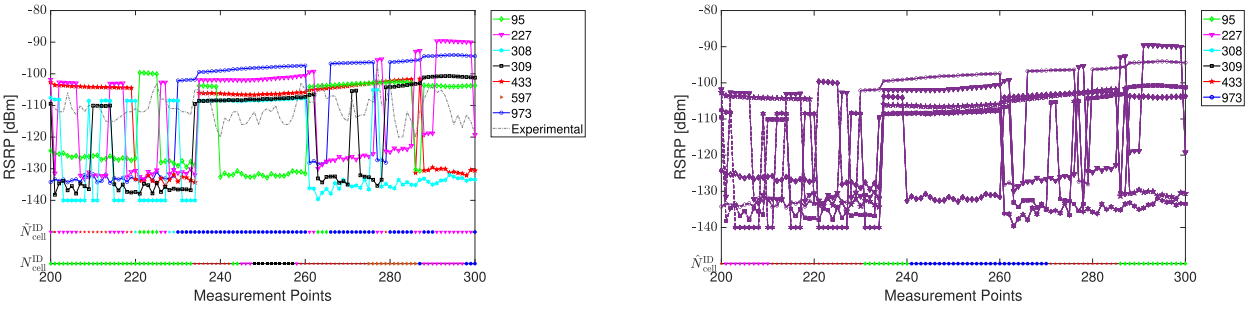

FIGURE 26. Comparison in the measurement interval from point 200 to point 300 between: (a) the experimental $N_{\text{cell}}^{\text{ID}}$ and without regression $\tilde{N}_{\text{cell}}^{\text{ID}}$ results and (b) our linear regression-based algorithm $\hat{N}_{\text{cell}}^{\text{ID}}$ results ($n_{\text{obs}} = 50$, $n_{\text{pred}} = 5$).

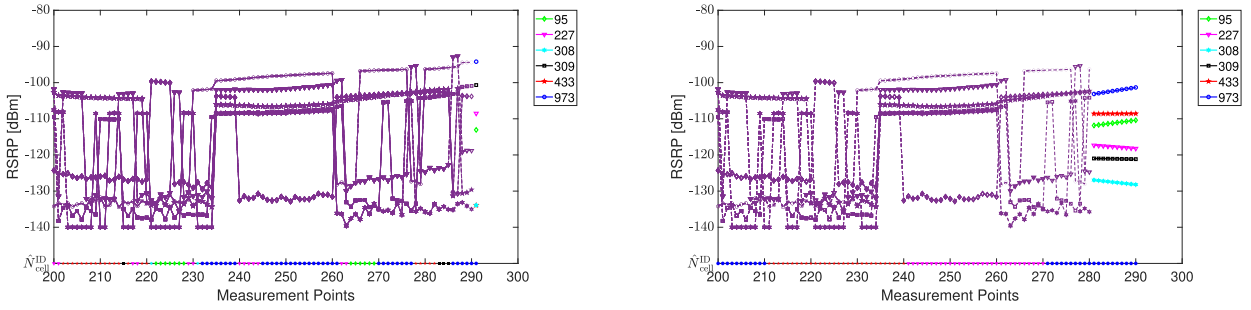

FIGURE 27. Comparison of $\hat{N}_{\text{cell}}^{\text{ID}}$ in the measurement interval from point 200 to point 300 between: (a) ($n_{\text{obs}} = 10$, $n_{\text{pred}} = 1$) and (b) ($n_{\text{obs}} = 100$, $n_{\text{pred}} = 10$).

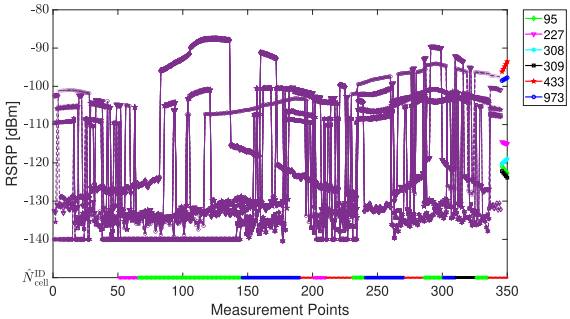

FIGURE 28. RSRP values linear regression-based identification of cell ID $\hat{N}_{\text{cell}}^{\text{ID}}$ along the considered path.

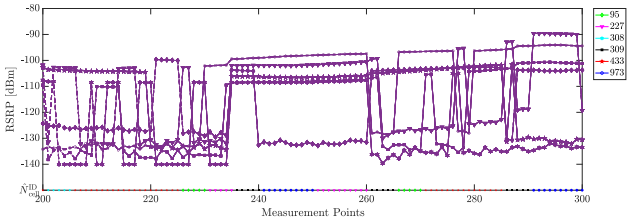

FIGURE 29. RSRP and distance-based second-order polynomial regression algorithm $\hat{N}_{\text{cell}}^{\text{ID}}$ results from point 200 to point 300.

Figure 23 and Figure 24. This unbalance of the cell IDs representation exacerbates when the dataset is not randomly split[3] into training and test subsets (for instance, using splitting percentages 70%-30% or 80%-20%), since in the

[3]The dataset split cannot be carried out in a random manner because we are dealing with sequential measurements.

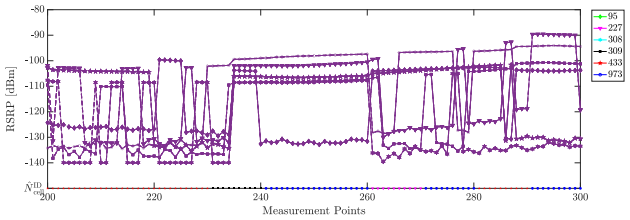

FIGURE 30. RSRP and distance-based logarithmic regression algorithm $\hat{N}_{\text{cell}}^{\text{ID}}$ results from point 200 to point 300.

last segment of the considered path only some of the six considered cell IDs were identified.

VIII. CONCLUSION

In this paper, we have implemented an experimental testbed to investigate the performance of a commercial 5G UE connected to a 5G public infrastructure. We have analysed the experimental data and we have shown that latency peaks and throughput drops are due to UHOs. In order to deal with UHOs, we have first developed a 5G NR DL transmission simulator which has then been used to test the performance of a novel UHO mitigation mechanism based on the linear regression of the measured CSI-RSRP values. It has been observed that, by using our RSRP-based linear regression approach, the number of avoided UHOs by a moving UE along a path is large and the number of performed HOs is minimized. Moreover, we have compared our proposed linear regression-based approach with (i) a second-order polynomial regression-based approach and (ii) a logarithmic regression-based approach. The observed results highlight how linear regression is computationally efficient, easy to implement, and, therefore, very attractive from a performance-complexity trade-off perspective. Using our approach, better QoS and QoE are perceived by the UE, as the UE since it experiences a lower latency and a higher throughput.

Future research activities will focus on different aspects: (i) evaluating the proposed UHOs mitigation mechanism on newly collected data in rural scenarios; (ii) comparing our approach with newly defined ones based on alternative ML and DL (e.g., NN) algorithms; (iii) evaluating the impact of real-world unpredictability (e.g., weather, obstructions) on the proposed Matlab simulator, and potential limitations introduced by the adoption of external software libraries (e.g., `iperf3`); and (iv) evaluating the behavior of the proposed UHO mitigation approaches in different contexts (e.g., urban, suburban, rural), as well as in the presence of high mobility scenarios.

ACKNOWLEDGMENT

An earlier version of this paper was presented in part at the European Wireless Conference, Rome, Italy, in October 2023.

REFERENCES

[1] *Third Generation Partnership Project (3GPP) Release 15*. Accessed: May 15, 2024. [Online]. Available: https://www.3gpp.org/specifications-technologies/releases/release-15

[2] R. Ali, Y. B. Zikria, A. K. Bashir, S. Garg, and H. S. Kim, "URLLC for 5G and beyond: Requirements, enabling incumbent technologies and network intelligence," *IEEE Access*, vol. 9, pp. 67064–67095, 2021, doi: 10.1109/ACCESS.2021.3073806.

[3] 5G Automotive Association (5GAA). *C-V2X Use Cases, Methodology, Examples and Service Level Requirements*. Accessed: May 15, 2024. [Online]. Available: https://5gaa.org/content/uploads/2019/07/5GAA_191906_WP_CV2X_UCs_v1-3-1.pdf

[4] A. U. Rehman, M. B. Roslee, and T. Jun Jiat, "A survey of handover management in mobile HetNets: Current challenges and future directions," *Appl. Sci.*, vol. 13, no. 5, p. 3367, Mar. 2023, doi: 10.3390/app13053367.

[5] A. Alhammadi, W. H. Hassan, A. A. El-Saleh, I. Shayea, H. Mohamad, and W. K. Saad, "Intelligent coordinated self-optimizing handover scheme for 4G/5G heterogeneous networks," *ICT Exp.*, vol. 9, no. 2, pp. 276–281, Apr. 2023, doi: 10.1016/j.icte.2022.04.013.

[6] M. Alhabo, L. Zhang, and N. Nawaz, "A trade-off between unnecessary handover and handover failure for heterogeneous networks," in *Proc. Eur. Wireless 23th Eur. Wireless Conf.*, Dresden, Germany, May 2017, pp. 1–6.

[7] J.-S. Kim and T.-J. Lee, "Handover in UMTS networks with hybrid access femtocells," in *Proc. 12th Int. Conf. Adv. Commun. Technol. (ICACT)*, vol. 1, Feb. 2010, pp. 904–908.

[8] R. Singoria, T. Oliveira, and D. P. Agrawal, "Reducing unnecessary handovers: Call admission control mechanism between Wimax and femtocells," in *Proc. IEEE Global Telecommun. Conf. GLOBECOM*, Houston, TX, USA, Dec. 2011, pp. 1–5, doi: 10.1109/GLOCOM.2011.6134137.

[9] K. Koutlia, B. Bojovic, Z. Ali, and S. Lagén, "Calibration of the 5G-LENA system level simulator in 3GPP reference scenarios," *Simul. Model. Pract. Theory*, vol. 119, Sep. 2022, Art. no. 102580, doi: 10.1016/j.simpat.2022.102580.

[10] T. R. Henderson, "Network simulations with the Ns-3 simulator," *SIGCOMM Demonstration*, vol. 14, no. 14, p. 527, 2008. [Online]. Available: http://conferences.sigcomm.org/sigcomm/2008/papers/p527-hendersonA.pdf

[11] S. Martiradonna, A. Grassi, G. Piro, and G. Boggia, "5G-air-simulator: An open-source tool modeling the 5G air interface," *Comput. Netw.*, vol. 173, May 2020, Art. no. 107151, doi: 10.1016/j.comnet.2020.107151.

[12] E. Oliosi, "Simulation-based analysis of experimental 5G NR downlink CSI-RSRP-based handover performance," in *Proc. Eur. Wireless Conf. (EW)*, Rome, Italy, 2023, pp. 1–6.

[13] B. H. Prananto and A. Kurniawan, "A new method to improve frequent-handover problem in high-mobility communications using RIC and machine learning," *IEEE Access*, vol. 11, pp. 72281–72294, 2023, doi: 10.1109/ACCESS.2023.3294990.

[14] D. Zidic, T. Mastelic, I. N. Kosovic, M. Cagalj, and J. Lorincz, "Analyses of ping-pong handovers in real 4G telecommunication networks," *Comput. Netw.*, vol. 227, May 2023, Art. no. 109699, doi: 10.1016/j.comnet.2023.109699.

[15] M. I. Goh, A. I. Mbulwa, H. T. Yew, A. Kiring, S. K. Chung, A. Farzamnia, A. Chekima, and M. K. Haldar, "Handover decision-making algorithm for 5G heterogeneous networks," *Electronics*, vol. 12, no. 11, p. 2384, May 2023, doi: 10.3390/electronics12112384.

[16] L. L. Vy, L.-P. Tung, and B. P. Lin, "Big data and machine learning driven handover management and forecasting," in *Proc. IEEE Conf. Standards for Commun. Netw. (CSCN)*, Helsinki, Finland, Sep. 2017, pp. 214–219, doi: 10.1109/CSCN.2017.8088624.

[17] S. Khunteta and A. K. R. Chavva, "Deep learning based link failure mitigation," in *Proc. 16th IEEE Int. Conf. Mach. Learn. Appl. (ICMLA)*, Cancun, Mexico, Dec. 2017, pp. 806–811, doi: 10.1109/ICMLA.2017.00-58.

[18] J. P. S. H. Lima, Á. A. M. de Medeiros, E. P. de Aguiar, E. F. Silva, V. A. de Sousa, M. L. Nunes, and A. L. Reis, "Deep learning-based handover prediction for 5G and beyond networks," in *Proc. IEEE Int. Conf. Commun.*, Rome, Rome, Italy, May 2023, pp. 3468–3473, doi: 10.1109/icc45041.2023.10279195.

[19] M. Behjati, M. A. Zulkifley, H. A. H. Alobaidy, R. Nordin, and N. F. Abdullah, "Reliable aerial mobile communications with RSRP & RSRQ prediction models for the Internet of Drones: A machine learning approach," *Sensors*, vol. 22, no. 15, p. 5522, Jul. 2022, doi: 10.3390/s22155522.

[20] S. K. Goudos, G. Tsoulos, and G. Athanasiadou, "Artificial neural network optimal modelling of received signal strength in mobile communications using UAV measurements," in *Proc. 12th Eur. Conf. Antennas Propag. (EuCAP)*, London, U.K., Apr. 2018, pp. 1–4, doi: 10.1049/cp.2018.1079.
[21] D. Karra, S. K. Goudos, G. V. Tsoulos, and G. Athanasiadou, "Prediction of received signal power in mobile communications using different machine learning algorithms: A comparative study," in *Proc. Panhellenic Conf. Electron. Telecommun. (PACET)*, Volos, Greece, Nov. 2019, pp. 1–4, doi: 10.1109/PACET48583.2019.8956271.
[22] L. Rokach, "Ensemble-based classifiers," *Artif. Intell. Rev.*, vol. 33, nos. 1–2, pp. 1–39, Feb. 2010, doi: 10.1007/s10462-009-9124-7.
[23] M. Schmahling, "Generation and analysis of 5G NR signals according to 3GPP," in *Proc. Electron. Design Innov. Conf. (EDI CON)*, Beijing, China, 2018, pp. 1–5.
[24] *Physical Channels and Modulation (Version 16.2.0, Release 16)*, Standard TS 38.211, 3rd Generation Partnership Project (3GPP), European Telecommunications Standards Institute (ETSI), Jul. 2020. [Online]. Available: https://www.etsi.org/deliver/etsi_ts/138200_138299/138211/16.02.00_60/ts_138211v160200p.pdf
[25] *Physical Layer Measurements (Version 16.2.0, Release 16)*, Standard TS 38.215, 3rd Generation Partnership Project (3GPP), Jul. 2020. [Online]. Available: https://www.etsi.org/deliver/etsi_ts/138200_138299/138215/16.02.00_60/ts_138215v160200p.pdf
[26] ASK Industries S.p.A. *Home Page*. Accessed: May 15, 2024. [Online]. Available: https://www.askgroup.global/
[27] J. Dugan. *Iperf3*. Accessed: May 15, 2024. [Online]. Available: https://iperf.fr/
[28] E. Dahlman, S. Parkvall, and J. Skold, "NR overview," in *5G NR*, 2nd ed., E. Dahlman, S. Parkvall, and J. Skold, Eds., New York, NY, USA: Academic, 2021, pp. 57–78, doi: 10.1016/B978-0-12-822320-8.00005-2.
[29] *Study on Channel Model for Frequencies From 0.5 to 100 GHz*, Standard TR 38.901, 3rd Generation Partnership Project (3GPP), European Telecommunications Standards Institute (ETSI), Jul. 2018. [Online]. Available: https://www.etsi.org/deliver/etsi_tr/138900_138999/138901/15.00.00_60/tr_138901v150000p.pdf
[30] D. S. Moore, W. Notz, and M. A. Fligner, *The Basic Practice of Statistics*, 6th ed., New York, NY, USA: W. H. Freeman and Company, 2013.
[31] *Handover Delay*, Standard TS 38.133, Section 6.1.1.2.1, 3rd Generation Partnership Project (3GPP), European Telecommunications Standards Institute (ETSI), Jul. 2019. [Online]. Available: https://www.etsi.org/deliver/etsi_ts/138100_138199/138133/15.06.00_60/ts_138133v150600p.pdf
[32] OpenStreetMap Foundation (OSMF). *OpenStreetMap*. Accessed: May 15, 2024. [Online]. Available: https://www.openstreetmap.org/
[33] G. A. F. Seber and A. J. Lee, *Linear Regression Analysis*, 2nd ed., Hoboken, NJ, USA: Wiley, 2003.

SUNIL MATHEW received the bachelor's degree in electronics and telecommunication engineering from Mahatma Gandhi University, India, in 2014, and the master's degree in communication engineering and the Ph.D. degree in information technologies from the University of Parma, Italy, in 2020 and 2023, respectively. He is currently a Research Associate with the Internet of Things (IoT) Laboratory, Department of Engineering and Architecture, University of Parma. His research interests include the IoT, 5G, and low-latency communication systems.

ELEONORA OLIOSI received the bachelor's degree (three-year program) in information, electronic, and telecommunication engineering and the master's degree (second cycle degree) in communication engineering from the University of Parma, Parma, Italy, in March 2018 and October 2020, respectively, with a thesis titled "Statistical Analysis of Sensor Data for Predictive Maintenance of Industrial Lyophilizers." She is currently pursuing the Ph.D. degree in automotive engineering for intelligent mobility with the University of Bologna, Bologna, Italy. She is also with the Internet of Things (IoT) Laboratory, University of Parma. Her research interests include 5G and autonomous driving.

LUCA DAVOLI (Member, IEEE) received the Dr.Ing. degree in computer engineering and the Ph.D. degree in information technologies from the Department of Information Engineering, the University of Parma, Italy, in 2013 and 2017, respectively. He is currently a non-tenured Assistant Professor with the Internet of Things (IoT) Laboratory, Department of Engineering and Architecture, University of Parma. He is also a Research Scientist at things2i Ltd., a spin-off of the University of Parma dedicated to the IoT and smart systems. His research interests include the IoT, pervasive computing, big stream, and software-defined networking.

NICOLÒ STROZZI received the master's degree in telecommunication engineering and the Ph.D. degree in information technologies from the University of Parma, Italy, in 2015 and 2019, respectively. Since 2019, he has been with the Antenna Department, ASK Industries S.p.A., as a Signal Processing Engineer. He is the author of several patents and articles. His main research interests include localization technologies, audio signal processing, and vehicular communication, such as V2X and 5G.

ANDREA NOTARI (Member, IEEE) received the master's degree (summa cum laude) in electronic engineering, in 2001. Since then, he has been with the Research and Development Antenna Department, ASK Industries S.p.A. In 2006, he became the Global Leader at the Antenna Department. He has coordinated several advanced projects in collaboration with automotive customers, universities, and research centers. He is the author of several patents, books, and articles. His main research interests include antenna designs, radio-frequency communications, and vehicular connectivity.

GIANLUIGI FERRARI (Senior Member, IEEE) received the Laurea (summa cum laude) and Ph.D. degrees in electrical engineering from the University of Parma, Parma, Italy, in 1998 and 2002, respectively. Since 2002, he has been with the University of Parma, where he is currently a Full Professor of telecommunications and the coordinator of the Internet of Things (IoT) Laboratory, Department of Engineering and Architecture. He is also the Co-Founder and the President of things2i Ltd. (https://www.things2i.com/), a spin-off of the University of Parma dedicated to the IoT and smart systems. His current research interests include signal processing, advanced communication and networking, the IoT, and smart systems. For more information: https://www.tlc.unipr.it/ferrari/.

Open Access funding provided by 'Università degli Studi di Parma' within the CRUI CARE Agreement